Alexandria Engineering Journal (2022) 61, 481–491

Alexandria University

Alexandria Engineering Journal

www.elsevier.com/locate/aej
www.sciencedirect.com

# Impact of artificial roughness variation on heat transfer and friction characteristics of solar air heating system

**Raj kumar [a], Rakesh Kumar [b], Sushil Kumar [c], Sashank Thapa [a], Muneesh Sethi [d], Gusztáv Fekete [e], Tej Singh [e,*]**

[a] *Faculty of Engineering and Technology, Shoolini University, Solan, H.P. 173229, India*
[b] *Department of Mechanical Engineering, Mahatma Gandhi Govt. Engineering College Kotla (Jeori), Himachal Pradesh 175018, India*
[c] *Department of Physics and Electronics, Hansraj College, University of Delhi 110007, India*
[d] *Dev Bhoomi Institute of Technology, Dehradun, Uttarakhand 248007, India*
[e] *Savaria Institute of Technology, Faculty of Informatics, ELTE Eötvös Loránd University, Szombathely 9700, Hungary*

Received 12 March 2021; revised 4 May 2021; accepted 14 June 2021
Available online 25 June 2021

**KEYWORDS**

Solar air heater;
Spacer length;
Friction factor;
Delta winglets

**Abstract** The present study describes the optimization of the spacer length parameter of perforated delta-shaped winglets (PDWs) imposed on the absorber plate of the solar air heater (SAH). An experimental set up is designed to analyze the influence of artificial roughness (AR) variation on the thermo-hydraulic performance of SAH. The variable parameter of the PDWs is the spacer length ($S_{pdw}$) which varies from0 mm to 300 mm in steps of 100 mm. The impact of variation of $S_{pdw}$ on Nusselt number ($Nu_{pdw}$), friction factor ($f_{rpdw}$) and thermo-hydraulic performance ($\eta_{pdw}$) is investigated. The fixed parameters of the PDWs are relative roughness height of perforated delta-shaped winglets = 0.8, relative longitudinal length of the perforated delta-shaped winglet = 2, relative transversal length of the perforated delta-shaped winglet = 0.66 and angle of incidence = 90°. The $Nu_{pdw}$ and $f_{rpdw}$of SAH provided with artificial roughened in the form of PDWs were improved by 5.17 and 4.52 times in comparison to SAH having smooth absorber plate. At the optimum value of spacer length$S_{pdw}$ = 0 mm and $Re$ of 12000, $\eta_{pdw}$ attains a maximum value of 3.14 (> 1). The study reveals the effectiveness of perforated delta winglets in the heat transfer augmentation of SAH.



## 1. Introduction

Life on earth is the manifestation of the energy. The energy consumption in the world has been increasing at an alarming

* Corresponding author.
E-mail address: sht@inf.elte.hu (T. Singh).
Peer review under responsibility of Faculty of Engineering, Alexandria University.

https://doi.org/10.1016/j.aej.2021.06.031

**Nomenclature**

| | |
|---|---|
| $L_{pdw}$ | Length of Test Section |
| $Nu$ | Nusselt number |
| $Nu_{ss}$ | Nusselt number of plain/smooth plate |
| $Nu_{pdw}$ | Nusselt number of perforated delta shaped winglet |
| $f_r$ | Friction factor |
| $f_{ss}$ | Friction factor of smooth plate, dimensionless |
| $f_{rpdw}$ | Friction factor of upstream perforated delta shaped winglet, dimensionless |
| $A_{apw}$ | Surface area of absorber plate with winglets |
| $Re$ | Reynolds number |
| $T_o$ | Air outlet temperature |
| $T_i$ | Air inlet temperature |
| $T_f$ | Bulk temperature |
| $V$ | Velocity of fluid |
| $B_{pdw}$ | Blockage ratio of upstream delta winglet |
| $P_{pdw}$ | Pitch ratio of upstream delta winglet |
| $\alpha_{pdw}$ | Angle of attack |
| $S_{pdw}$ | Spacer length |
| $\eta_{pdw}$ | Thermo hydraulic efficiency |
| $Q_{pdw}$ | Useful heat gain |
| $h_{pdw}$ | Heat transfer coefficient |
| k | Thermal conductivity of air |
| $m_{pdw}$ | Mass flow rate (MFR) |
| SWH | Solar water heater |
| SAH | Solar air heater |
| $\Delta_{pdw}$ | Pressure drop |
| HTR | Heat transfer rate |
| HTE | Heat transfer enhancement |
| TP | Thermo-hydraulic performance |
| PDWs | Perforated delta shaped winglets |

rate for the past few decades. Energy sources like coal, wood, petrol, diesel and natural gas are depleting. So, emphasis is given to search alternative resources which could produce power in sustainable way by means of creating less waste and lowering carbon dioxide emission [1,2]. The renewable energy is nurtured from ample resources such as sun light, wind, rain, tides etc. India is one of 121 countries having natural solar energy blessings. The absorber tube in solar air heater (SAH) absorbs sun light and gets heated [3]. Then this heat is transferred to the fluid. Turbulence promoters in the form artificial roughness (AR) are used for heat transfer augmentation. The AR is characterized in terms of relative winglets height, relative winglets pitch, open area ratio, circularity, angle of incidence and spacer length [3–5]. Warrier and Kotebavi [6] carried out investigation on thermal enhancement of SAH with delta winglet attached to the absorber plate. The authors reveal substantial impact of position of the winglets and angle of incidence on heat transfer rate (HTR). Nusselt number ($Nu$) rises 150% and friction factor ($f_r$) decreases 200% resulting 1.4 times enhancement in heat transfer. Maithani et al. [7] investigated heat transfer augmentation using wavy winglets on the absorber plate. They found fall in $f_r$ with rise in $Re$. Promvonge et al. [8] examined impact of both ribs and delta-winglets (DWs) on heat transfer enhancement. The obtained results show that $Nu$ and $f_r$ values for this geometry were greater than those for the rib and DWs alone. At low angle of incidence, the used geometry gives enhanced heat transfer and better thermal performance (TP). Promvonge and Skullong [9] investigated the TP of heat exchanger duct fitted with Perforated Winglets. They have obtained significant increase in the $Nu$ and decrease in the $f_r$ using this geometry. Sawhney et al. [10] investigated $Nu$ and $f_r$ losses for wavy DWs fitted on absorber plate of the SAH. At optimum geometry parameters, the thermohydraulic performance of 2.09 was obtained. Singh et al. [11] developed a SAH provided with serpentine wavy channel. The authors have studied the influence of variation of geometrical parameters on the TP. The optimization of geometrical parameters was done using decision making technique and exergy analysis. They obtained enhancement in the TP with increase in the mass flow rate (MFR). Skullong et al. [12] investigated SAH provided with wavy-groove and delta-winglet vortex generators (DWVG) as roughness. The $Re$ was changed from 4800 to 23,000 depending upon the hydraulic diameter of the duct. Skullong et al. [13] studied SAH having winglet-type vortex generators (WVG) pasted on the bottom of heated plate experimentally and numerically. The experimental results infer that the WVG with blockage ratio (BR) = 0.48 and pitch ratio (PR) = 1 improve the enhancement in $Nu_{rs}$ and $f_{rs}$as compared with the smooth duct. Warrier and Kotebavi [14] compared the experimental and numerical results for SAH with DWVG underside the absorber plate with punched holes. The experimental and numerical results were compared which indicated heat transfer enhancement of 20–150%. Chompookham et al. [15] analyzed the impact of both wedge ribs and WVGs on $Nu_{rs}$ and $f_{rs}$ of solar air channel. The $Nu_{rs}$ and $f_{rs}$ results obtained for this configuration were found to superior than the results for ribs/WVGs alone. Torii et al. [16] examined the $Nu_{rs}$ and $f_{rs}$ of a heat exchanger (fin-tube) with circular tubes by installing DWVG. They obtained improvement in the $Nu_{rs}$ and decrease in the $f_{rs}$ with $Re$ changing from 350 to 2100. Yakut et al. [17] examined the $Nu_{rs}$ and $f_{rs}$, for tapes with double-sided DWs under distinct geometrical and stream parameters. Taguchi experimental-design method was used for determination of optimum parameters of the turbulator. The optimum outcomes for $Nu_{rs}$ and $f_{rs}$ were obtained at $Re$ of 16906, $P_b$ of 25 mm, $H_b$ of 8 mm and $\alpha_a$ of 30°. Skullong et al. [18] experimentally analyzed the TP of a SAH with combined wavy-groove and DWVG. At the optimum parameters, they have obtained $Nu_{rs}$ and $f_{rs}$ around 6 and 30 times higher than smooth SAH. Kotcioglu et al. [19] investigated the entropy generation of a winglet-type convergent-divergent longitudinal vortex generator. The $Nu_{rs}$ was found to rise with raise in the cross-stream velocity. The analysis outcome shows that the vortex generator is effective in improving disorderly mixing of fluid. Eiamsa-ard et al. [20] experimentally studied the influence of delta-winglet twisted tape (DWT) on the $Nu_{rs}$ and $f_{rs}$. Authors detected the effectiveness of oblique DWT in providing superior $Nu_{rs}$ as compared to straight DWT. Appreciable improvement in $Nu_{rs}$,$f_{rs}$ and $h_t$ with the

O-DWT are obtained as compare to typical twisted tape. Handoyo et al. [21] studied numerically the influence of obstacles spacing inserted in the channel of a SAH on $Nu_{rs}$ and $f_{rs}$. At optimum value of obstacle spacing $Nu_{rs}$ and $f_{rs}$ are found to be 3.46 and 19.9 times higher than those for smooth channel. Ghalambaz et al. [22] examined the unstable heat transfer (HT) behavior of the nano-encapsulated phase change materials (PCM) in the coaxial pipe. The effect of the nano-encapsulated PCMs volume fraction, Stefan number (Ste), Rayleigh number (*Ra*) as well as the fusion temperature of the nanoparticles on the charging and discharging of the nano-encapsulated PCM was investigated. Results show that *Nu* decreases with increase in Ste during charging mode but in discharging mode *Nu* is independent of Ste. Also the particles fusion temperature ($\theta_f$) affects the HT of the system which basically depends on the working mode of the system. The results suggested that for Ste = 0.2, Ra = $10^6$ and $\theta_f$ = 0.1 the Nu increased about 1.73 for the melting of the core nano-encapsulated PCM particles and 1.55 times for the solidification of the core nano-encapsulated PCM particles. Zadeh et al. [23] scrutinized the effect on the HT enhancement of the circular latent heat thermal energy storage (LHTES) system by adding copper foam and the nano additives. The results showed that the Cu foam with additives Cu/GO was more effectual than each enhancement method was used separately. The results pointed out that the charging power of the LHTES system can be improved about 4 times by using Cu foam with nano additives as compared to using PCMs. Ghalambaz et al. [24] analyzed the convective HT of the suspension of the NEPCM in an inclined porous cavity. The influence of Ste and $\theta_f$ on the HT characteristics and heat capacity ratio was examined for the angle of inclination of the cavity. The resulted concluded that the optimum HT performance was attained for $\theta_f$ = 0.5 and angle of inclination of 42°and by decreasing Ste the heat transfer increases. Mehryan et al. [25] conducted an experiment by using local thermal non-equilibrium model to study the natural convection of the Ag-MgO/water nanofluid present inside the porous enclosure. Darcy model was used to investigate the flow inside the porous medium. The main parameters such as Ra, porosity, volume fraction of the nanoparticles and HT coefficient were studied. The results demonstrated that by diffusing the Ag-MgO nanofluid in the base fluid water reduces the HT between the two phases of porous enclosure. Ghalambaz et al. [26] analyzed the conjugate convection flow of the Ag-MgO/water nanofluid in a square cavity. The effect of the deviation of the key parameters such as volume fraction of the nanoparticles, *Ra* as well as the ratio of thermal conductivity of wall and nanoparticles were examined. The results pointed out that the HT increases by adding nanoparticles for low Ra number whereas for high *Ra* number the *Nu* at the surface of wall decreases. Chamkha et al. [27] studied the flow of natural convection of the working fluid in the uniform porous medium sustained by a transparent vertically flat plate due to the solar radiation. Boussinesq approximation was used to derive the boundary conditions. At the flat surface, convection boundary conditions are used. The graphical results were demonstrated for the temperature and velocity fields whereas the Nu and boundary friction was also discussed. Parvin et al. [28] directed the numerical simulation of the laminar flow of the natural convection in an annulus that contains the water and alumina nanofluid. The annulus outer surface was kept at constant temperature $T_c$ whereas the inner part was equivalently heated. The HT enhancement in an annulus was investigated by the help of two conductivity model i.e. Chon and Maxwell model. The effect of the nanoparticles, Prandtl number and Grashof number on the HT characteristics was examined. The results showed that by increasing the volume fraction of the nanoparticles and the Prandtl number, significant enhancement in the HT was observed. Chamkha et al. [29] studied the influence of the solar radiation on the natural convection flow of air present inside the semi finite vertical plate. The boundary layer equation was solved numerically by reducing equation to the non-similar forms. The effect of the parameters such as Schmidt number, solar radiation, and the distance from the edge of semi vertical plate was presented in the solution and examined. Manokar et al. [30] performed an experiment to analyze the effect on the enhancement of the freshwater productivity of the active inclined solar panel basin solar still integrated with flat plate collector. The maximum productivity of the freshwater attained at mass flow rate ($m_f$) of 1.8, 3.2, 4.8 was 7.5, 6.5 and 4.7 kg/h. The results suggested that by increasing $m_f$, the freshwater productivity as well as the overall thermal efficiency and exergy η also increases. Basha et al. [31] investigated the effect of the solar radiation and the induced MF on the forced convective flow of the Single-Walled Carbon NanoHorn (SWCNH)/diamond-ethylene as well as the water nanofluid over the wedge, stagnation point and the plate. The governing equations were changed into differential equations by using the similarity transformation and solved numerically. The Boit number, magnetic parameter, Prandtl number and radiation parameter was represented graphically. The results suggested that temperature of the wedge, stagnation point, and plate was enhanced by increasing the volume fraction of SWCHN/diamond-ethylene nanofluid. Sasikumar et al. [32] detected a study on passive inclined solar panel basin still at different MFR. The experimental results show that increasing the MFR results in decreasing the temperature of water and panel. Representing that temperature is directly proportional to the solar panel basin still productivity, however panel temperature is inversely proportional to the PV panel production and efficiency. The collected freshwater at different ($m_f$) is 4.68, 7.56 and 10.08 $kg.h^{-1}$ with daily productivity of 3.7, 2.7, and 1.6 kg. Also at higher flow condition, the still energy and exergy efficiency decreases, and it is observed as 36.06, 25.56 and 16.95% and 2.97, 1.91 and 1.01%, respectively, for flow rates of 4.68, 7.56 and 10.08 $kg.h^{-1}$. The electrical, thermal and exergy efficiency of photovoltaic panel increases under higher flow condition and it is found as 8.05, 8.81 and 9.44%, 11.43, 20.8 and 22.17 and 19.38, 20.58 and 21.16% for MFR of 4.68, 7.56 and 10.08 $kg.h^{-1}$. Paraschiv et al. [33] carried out an economic examination of solar air heater (SAH) incorporated in residential building wall to enhance the energy η by providing insulation and achieving heat gain. The annul energy η of the SAH was investigated throughout the year in both cold and warm climatic conditions. The performance of the suggested SAH was compared with gas boiler heating system. The results pointed out the payback time of the proposed SAH will recover approximately between 5 and 14 years when the subsidies provided by the government are between 0 and 50%. Long et al.[34]conducted an experiment by combining the solar hot water (SHW) and air source heat pump (ASHP) and analyzed their performance by connecting them in series, parallel as well as preheating connection of

SHW and ASHP. Their efficiency performance was examined during the winter season. It was concluded that the solar radiation intensity and the surrounding temperature was the major influence on theenergy η on all the type of connection in which the SHW and ASHP was connected. The graphical results are showed for the energy η for all the three-above connection of ASHP and SHW. Teamah et al. [35] presented a complete review of the applications of PCM in residential heating. Various studies accounting for research methodology, structural characterization and their performances in long terms were analyzed. The research gaps were highlighted in the paper and technical gaps pointed out the further research must be focused toward enhancing properties of PCM for domestic uses and incorporation of the PCM in the different systems. Teamah et al. [36] carried out a numerical simulation and non-dimensional investigation of the dynamic performance of Thermal energy storage (TES) tank containing PCM. The numerical model using enthalpy-porosity method was established and their results are checked against the experimental results. The energy gain in TES system was compared with sensible heat storage system. The results suggested that the energy gain of 179% was attained for 50% packing ratio and at 10 °C working temperature in water tank. Teamah et al. [37] conducted a numerical analysis of electrical load shifting ability of ground source heat pump system with PCM that store the thermal energy. The amount of thermal shielding required by the shifting the HP process during peak time was examined. The results suggested that the allover electric shift to off peak hour was attained by $2.5/1m^3$ of water tank having 50% of PCM by volume. It was concluded that the higher storage capacity can be attained by limiting the temperature working range of the constituted hybrid system. The studies [38–43] incorporated the heat transfer enhancement and friction factor in SAH and solar water heater.

The literature review shows that numerous studies have been carried out to investigate the TP of SAH with roughened channel. The roughness was provided by rib, baffle, dimple, protrusion, rind and blocks over the absorber plate. Use of perforated type AR as a turbulence promoter on absorber plate in a SAH has found to be an effective technique for heat transfer augmentation. The arrangement of the winglets is represented in terms of spacer length. When winglets are fixed on entire length regularly then spacer length is zero. When set of winglets are fixed in irregular manner means smooth surface of length 100 mm, 200 mm and 300 mm is inserted between the consecutive set of winglets, then spacer length is taken 100 mm, 200 mm and 300 mm respectively. This length of smooth surface between consecutive set of winglets is called spacer length. The randomness in arrangement of winglets causes improper mixing of fluids. The aim of present paper is to investigate the influence of spacer length of perforated delta shaped winglets on the heat transfer and friction factor characteristics of SAH.

## 2. Experimental set-up

The examinational set up used in the present work has PDWs as a turbulence promoter fitted to the under-side of one broad wall as artificial roughness. The experimental data obtained is presented in the form of $Nu_{pdw}$ and $f_{rpdw}$ plots as function of geometrical parameters of perforated delta shaped winglets. The various parameters of PDWs are relative roughness height of perforated delta-shaped winglet, relative longitudinal length of the perforated delta-shaped winglet, relative transversal length of the perforated delta-shaped winglet, angle of incidence, spacer length ($S_{pdw}$) and Reynolds number ($Re$). Fig. 1 shows the schematic representation of the indoor experimental set-up.

This is an open loop system having rectangular channel, variable transformer (Variac), temperature indicator, anemometer, micro-manometer, gate valves, centrifugal blower, GI pipe and thermocouples. Rectangular channel have an entrance-section, a test section and an exit-section. This is coupled to the suction side of centrifugal blower. Atmospheric air passing through the rectangular channel flows beneath the absorber plate. The electrical heater assembly provides constant heat flux to the absorber plate. The energy gained by absorber plate is controlled by Variable transformer. The copper constantan thermocouples (CCT) measures air temperature at entrance and exist of the test section. MFR $\left(m_{pdw}\right)$ of the air is measured with anemometer. A micro manometer used to measure the $f_r$. The gate valves attached to the centrifugal blower are used to vary the flow rate through the test section.

### 2.1. Elements of experimental set-up

#### 2.1.1. Solar air heater channel

The experimental channel (Fig. 2) consists of a rectangular wooden channel of dimension $30cm \times 3cm \times 200cm$ having entrance section $50cm$, test section $120cm$and exit section of length $30cm$with channel aspect ratio (W/H) of 10.

The bottom portion of the SAC has been prepared with 2 cm thick wooden plank and 0.6 cm thick plywood attached on it. A laminated mica sheet of thickness 1 mm is pasted on top of the plywood to provide a high-quality smooth surface. The side walls of the channel are made up of 2.5 cm wooden plank with 0.15 cm thick mica pasted on the inner side.

#### 2.1.2. Heat flux generator

An electric heater is used for generating radiation flux equivalent to solar radiations in the experimental investigation. The electric heater of dimension $120cm \times 30cm$ was fabricated with nichrome wire in series and parallel. For testing of SAH, a constant heat flux of 1000 $W/m^2$is provided to the absorber plate by a Variac. The wires are attached on asbestos sheet of thickness$0.4mm$. For uniform distancing and prevention of back heating strip of Mica is used in place of asbestos sheet. Glass wool layer of thickness 9 cm is used at backside of the heater to reduce heat losses. For insulating top of heater assembly, a wooden sheet having thickness of 1.2 cm is used.

#### 2.1.3. Air handling equipment

The centrifugal blower (Fig. 3a) sucks atmospheric air with the help of an AC motor. The outlet of the rectangular channel is coupled to the centrifugal blower through $8cm$ diameter pipe. The flow of air is controlled with the help gate valves provided at entrance side and exit side of the blower. The vibrations transmitted from blower to the rectangular channel are reduced by coupling control valves and the orifice plate assembly with flexible PVC pipe. The seals and gaskets are used to

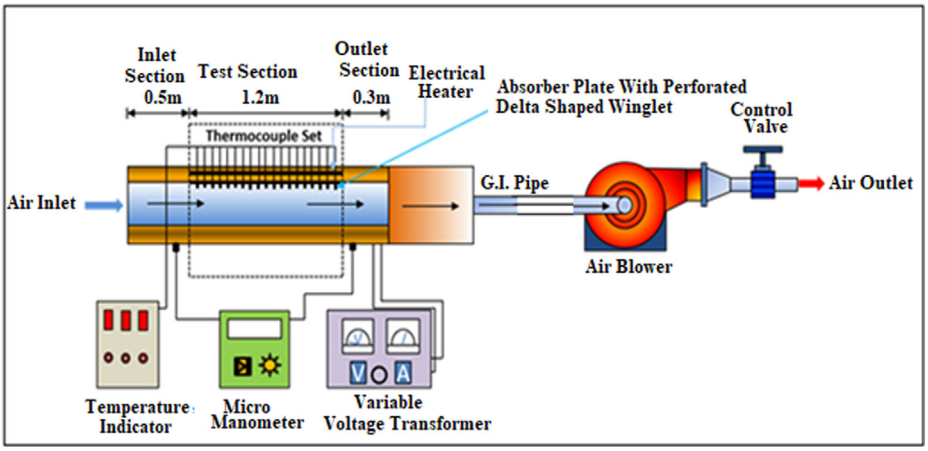


**Fig. 1** Schematic diagram of the experimental set-up.

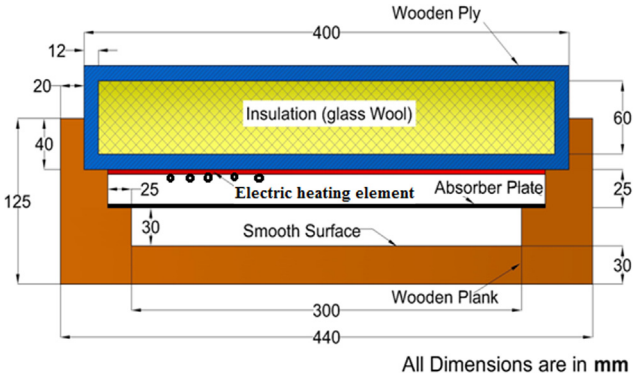


**Fig. 2** Cross-sectional view of the channel.

prevent air leakages from the connecting joints of the system. The leakage checking is done by applying soap solution at joints.

### 2.1.4. Perforated delta-shaped winglet absorber plate

An Aluminium sheet of size $120cm \times 30cm \times 0.2cm$ is used as an absorber plate. The perforated delta-shaped winglets are provided on the Aluminium sheet to produce turbulence to produce artificial roughness. Winglets are made by thin Aluminium sheet of thickness 0.7 mm. The perforated delta-shaped winglets side of the plate is on the inner side of the rectangular channel of the test section. Fig. 3b shows the schematic view of perforated delta-shaped winglet.

This plate is heated from the upper side through heater assembly and thus subjected to a constant heat flux. The parameters of perforated delta-shaped winglets have been expressed as, relative roughness height of perforated delta-shaped winglet ($e_d/H_D$), relative longitudinal length of the perforated delta-shaped winglet ($P_{lpdw}/b_d$), relative transversal length of the perforated delta-shaped winglet ($P_{tpdw}/b_d$), angle of incidence ($\alpha_{pdw}$) and spacer length ($S_{pdw}$) in mm. Out of these parameters of PDWs only spacerlength have dimension and all other are dimensionless. The range of perforated delta-shaped winglets roughness is given in Table 1. The spacer length is schematically represented in the Fig. 4.

## 2.2. Instrumentation of experimental set-up

### 2.2.1. Temperature measurement

Temperature of the ambient air and absorber plate are measured by means of a calibrated CCT with accuracy of $\pm$ 0.01°C with temperature measurement range of 0 – 400°C [44]. The temperature in the rectangular channel is measured with 29 CCTs (3, 5 and 21 for measurement of inlet

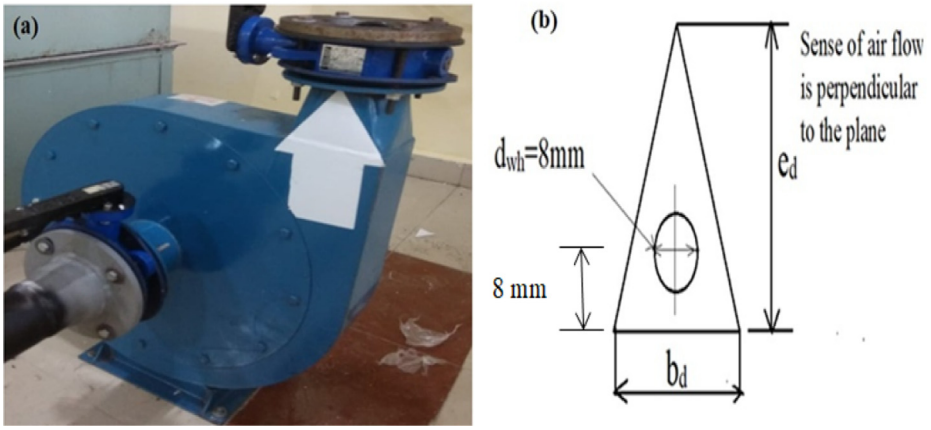


**Fig. 3** (a) Photographic view of the centrifugal blower, (b) Schematic view of perforated delta-shaped winglet.

**Table 1** Data of flow and roughness of parameters.

| Operating parameters | Symbols | Range |
|---|---|---|
| Relative roughness height of perforated delta-shaped winglets | $e_d/H_D$ | 0.8 |
| Relative longitudinal length of the perforated delta-shaped winglets | $P_{lpdw}/b_d$ | 2 |
| Relative transversal length of the perforated delta-shaped winglets | $P_{tpdw}/b_d$ | 0.66 |
| Spacer Length | $S_{pdw}$ | 0–300 mm |
| Angle of incidence | $\alpha_{pdw}$ | 90° |
| Reynolds number | $Re$ | 2000–12000 |

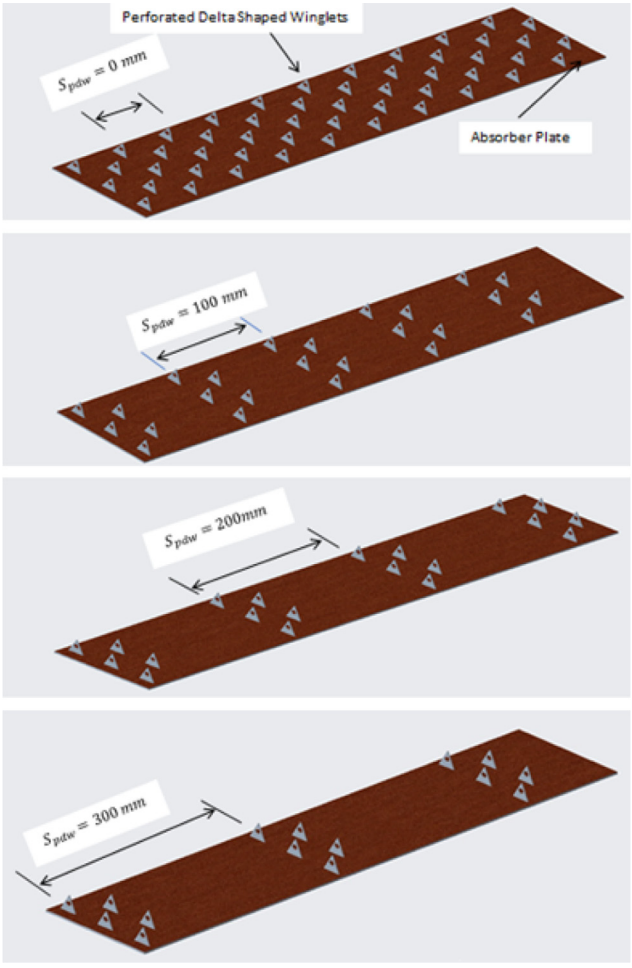


**Fig. 4** Schematic diagram of spacer length.

air, outlet and absorber plate temperature respectively). Fig. 5 schematically represents the location of CCTs in the rectangular channel.

### 2.2.2. Air flow measurement and channel pressure drop measurement

The rate of flow of air through the rectangular channel of SAH is measured with a digital anemometer. The anemometer used if of vane type and having a resolution of 0.1. The electronic micro-manometer has used for measurement of pressure drop across the rectangular channel. The perforated delta-shaped winglets (PDW) mounted on the absorber plate lead to drop in the pressure. Electronic micro-manometer having measuring range of $\pm 100Pa$ and least count of $0.1Pa$ is used for pressure measurement.

### 2.2.3. Experimental procedure

The calibration of measuring instruments has been done before commencing the experiment. The soap solution is applied on the joints to ensure leak free joints and voltage on Variac is fixed to generate an equivalent flux as that of sun ($1000W/m^2$). Centrifugal blower is switched on and the necessary arrangements are done to provide predetermined MFR of the air through the channel and power input to the heater. A fixed voltage to the heater plate is insured by using a voltage stablizer. The tempertaure have been measured 6 times in a hour to confrm the steady state condition. It has been found that steady state condition is achieved in 2–3 h in winter days. After noticing the various parameters when the mass flow rate is changed then it takes about one hour for equilibrium condition. The parametric values of perforated delta winglets mounted on the absorber plate used in experiment are relative roughness height($e_d/H_D = 0.8$), relative longitudinal length ($P_{lpdw}/b_d = 2$), relative transversal length ($P_{tpdw}/b_d = 0.66$), angle of incidence ($\alpha_{pdw} = 90°$), spacer length ($S_{pdw} = 0, 100\text{mm}, 200\text{mm}, \&300mm$) and Reynolds number ($Re$ = 2000–12000).Several observations for air and absorber plate temperature at distinct locations in the channel have been recorded at various parametric values of PDWs ($S_{pdw}$rangesfrom0to300mm) and $Re$ ranges from 2000 to 12000, while the other parameters are kept constant. Utilizing this idea, 4 absorber plates roughened with perforated delta-shaped winglet are fabricated and tested in the present investigation.

## 2.3. Data reduction, validation and uncertainty analysis

The heat transfer ($h_t$),$Nu_{pdw}$ and $f_{pdw}$ have been computed from the data collected. The relations used for the computation of these parameters are given below (Eqs. (1)–(9)). The plate mean temperature is taken as the average temperature recorded by thermocouples as:

$$T_p = \frac{\sum T_i}{N}, wherei = 1 - 21andN = 21 \quad (1)$$

The mean bulk air temperature $T_f$ is average of inlet ($T_i, i = 1$) and outlet ($T_o$) temperatures,

$$T_f = \frac{T_i + T_o}{2} \quad (2)$$

Velocity of air through channel is computed as:

$$V = \frac{m_{pdw}}{\rho_a WH} \quad (3)$$

Where $m_{pdw}$ is MFR of the air, has been measured from anemometer and $\rho_a$ is density of air.

The hydraulic diameter of channel is,

$$D_{hd} = \frac{4.(W.H)}{2.(W+H)} \quad (4)$$

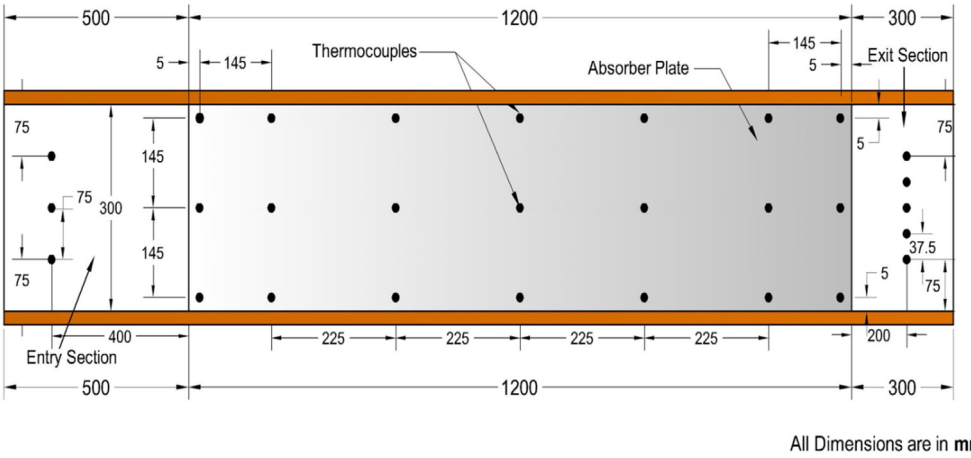


**Fig. 5** Thermocouple position in the rectangular channel.

Reynolds number ($Re$) of air stream in the channel is,

$$Re = \frac{V.D_{hd}}{v} \tag{5}$$

Heat transfer rate $Q_{pdw}$ from absorber to the air is,

$$Q_{pdw} = m_{pdw}c_p(T_0 - T_i) \tag{6}$$

The heat transfer coefficient ($h_{pdw}$) for test section is,

$$h_{pdw} = \frac{Q_{pdw}}{A_{ap}.(T_p - T_f)} \tag{7}$$

The Nusselt number($Nu_{pdw}$) is related to $h_t$ as:

$$Nu_{pdw} = \frac{h_{pdw}D_{hd}}{K_a} \tag{8}$$

The pressure drop $(\Delta_p)_d$ across the test section length is related to friction factor ($f_{rpdw}$) by Darcy equation as:

$$f_{rpdw} = \frac{2(\Delta_p)_d D_{hd}}{4\rho_a L_{pdw} V^2} \tag{9}$$

The experimental data of $Nu_{ss}$ and $f_{ss}$ recoded for a smooth channel have been compared with theoretical predictions. The theoretical data for $Nu_{ss}$ and $f_{ss}$ [45] is obtained from Dittus-Boelter equation (Eq.10) and modified Blasius equation (Eq.11) respectively and used for validation of test data.

Dittus-Boelter equation is:

$$Nu_{ss} = 0.023Re^{0.8}Pr^{0.4} \tag{10}$$

Modified Blasius equation is:

$$f_{ss} = 0.085Re^{-0.25} \tag{11}$$

The comparison between predicted and experimental results is shown in Fig. 6. The data obtained from the experimental measurements might be contradictory from its real values due to the occurrence of random errors. Therefore, it is essential to measure the maximum probable error during the experiment. An error examination has been performed based on the interpretations of raw data used to determine the uncertainty in experimental outcomes. The approach proposed by Kline and McClintock [46] is employed in present work to determine the change in provisional results. The methodology adopted for calculating experimental uncertainty in the measurement of $Nu_{pdw}$, $Re$, $f_{pdw}$, and $\eta_{pdw}$ is presented in Appendix A.

## 3. Results and discussion

The aim of the current study is to investigate impact of variation in the parametric values of PDWs mounted over the absorber plate, on the heat transfer augmentation. The $Q_{pdw}$ to the air can be considerably improved because of perforated delta-shaped winglet that creates turbulence in the stream. From past studies it can be concluded that artificial roughness in the solar air channel improve heat transfer coefficient. The artificial roughness also cause rise in the friction factor which result in the requirement of high pumping power to maintain stream in the channel. Therefore, the roughness parameters should be optimized to keep lowest friction factor and highest heat transfer coefficient with higher thermo hydraulic efficiency. In the present manuscript randomness in the arrangement of the winglets is represented in terms of spacer length. When winglets are fixed on entire length regularly then spacer length is zero. When set of winglets are fixed in irregular manner means smooth surface of length 100 mm, 200 mm and 300 mm is inserted between the consecutive set of winglets, then spacer length is 100 mm, 200 mm and 300 mm. This length of smooth surface between consecutive set of winglets is called spacer length. The irregularly of randomness in fixation of winglets is defined in terms of space length. The randomness in arrangement of winglets causes improper mixing of fluids.

### 3.1. Heat transfer characteristics

Fig. 7 shows change in $Nu_{pdw}$ with $Re$ at selected values of $S_{pdw}$. The graph clearly show increase in the heat transfer with the attached of PDWs on the absorber plate of SAH. From the experiment it is concluded that PDWs with $S_{pdw}$ = 0 mm (winglets are fixed on the entire length of the absorber plate) shows maximum enhancement in the HFR.

The experimental findings show that spacer length of the PDWs strongly influences the HTR. The experiment is con-

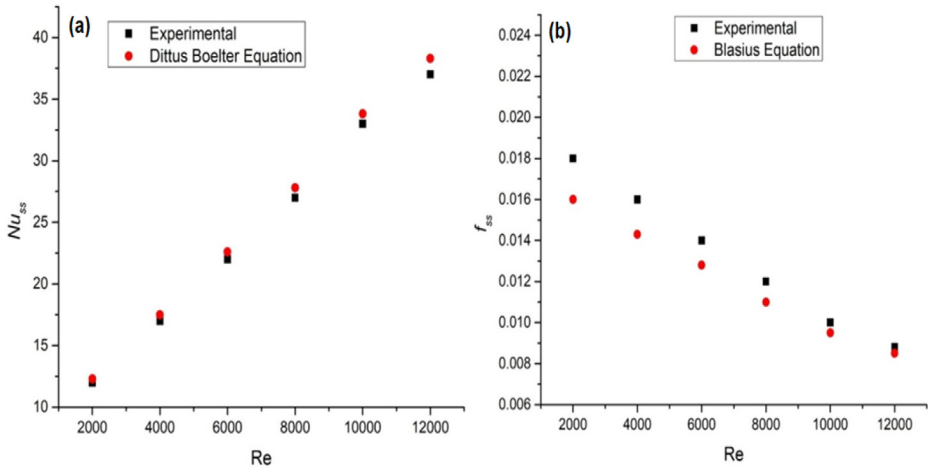


**Fig. 6** Comparison of experimental and predicted data of (a) $Nu_{ss}$ and (b) $f_{ss}$.

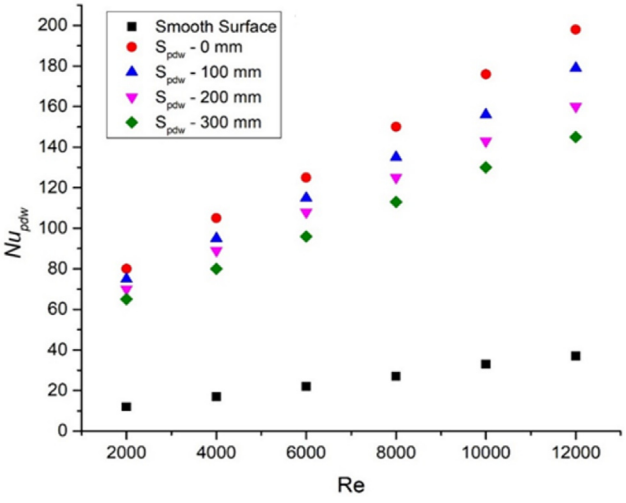


**Fig. 7** Variation of $Nu_{pdw}$ with $Re$ at different $S_{pdw}$.

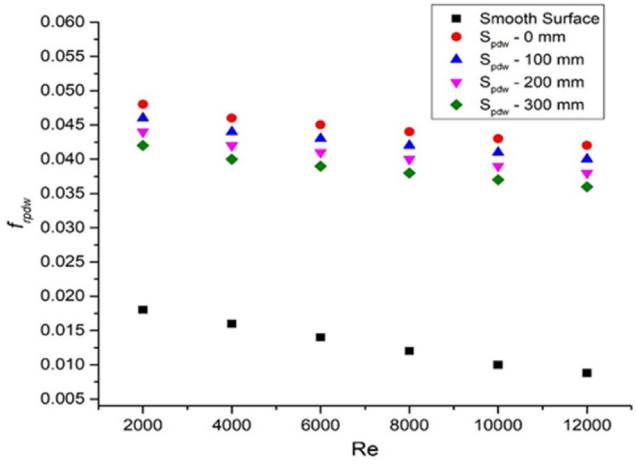


**Fig. 8** Variation of $f_{rpdw}$ with $Re$ at different $S_{pdw}$.

ducted at 4 different values of spacer length starting from 0 mm to 300 mm with step of 100 mm. At$S_{pdw}$ = 100 mm, the turbulence intensity of the flow drops and caused fall in $Nu_{pdw}$. Further rise in $S_{pdw}$ of perforated delta shaped winglets causes less turbulence. So the flow of the air become fast, and heat transferred to the air will be less leading to decrease in $Nu_{pdw}$. At$S_{pdw}$ = 0 mm, proper mixing of fluids take place and fluid receives maximum heat. So HTR is optimum for the geometry having PDWs on the entire length of the absorber plate.

### 3.2. Friction factor characteristics

The dependence of $f_{rpdw}$ on $Re$ at distinct values of $S_{pdw}$ is depicted in the Fig. 8. The spacer length of the delta shaped winglets have considerable impact on the heat transfer augmentation. After entering the rectangular channel, the air faces obstructions due to the presence of PDWs attached on the absorber plate of SAH. The perforated delta-shaped winglets produce turbulences and reduce the flow of air resulting in sufficient heat transfer to air from the absorber plate. These obstructions also cause increase in the friction. The repeated hindrances result in enhanced heat transfer but also increased $f_{rpdw}$. With increase in the spacerlength, the obstructions in the flow of air decreases causing less $f_{rpdw}$

### 3.3. Thermo-hydraulic performance

As discussed in Section 3.2, the spacer length of the delta shaped winglets have considerable impact on the heat transfer augmentation. The perforated delta-shaped winglets produce turbulences and reduce the flow of air resulting in sufficient heat transfer to air from the absorber plate. The repeated hindrances result in enhanced heat transfer but also increased $f_{rpdw}$. With increase in the spacerlength, the obstructions in the flow of air decreases causing less $f_{rpdw}$. The desired geometry must result in maximum enhancement in heat transfer and lowest penalty of rise in friction factor. So to measure the efficiency of solar air heater, the researchers [47] proposed a criterion represented by thermo-hydraulic performance ($\eta_{pdw}$) and is calculated by using following equation:

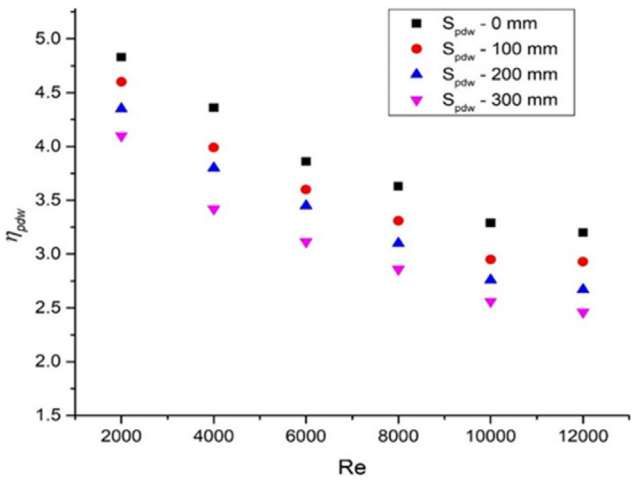


**Fig. 9** Variation of $\eta_{pdw}$ with $Re$ at different $S_{pdw}$.

$$\eta_{pdw} = \left(Nu_{pdw}/Nu_{ss}\right)/\left(f_{rpdw}/f_{ss}\right)^{0.33} \quad (12)$$

Fig. 9 shows the variation of $\eta_{pdw} = \left(Nu_{pdw}/Nu_{ss}\right)/\left(f_{rpdw}/f_{ss}\right)^{0.33}$ with $S_{pdw}$ (0 to 300 mm) for distinct values of $Re$ and constant parametric values such as relative roughness height $(e_d/H_D) = 0.8$, relative longitudinal length of the perforated delta-shaped winglet $(P_{tpdw}/b_d) = 2$, relative transversal length of the perforated delta-shaped winglet $(P_{tpdw}/b_d) = 0.66$, angle of incidence $(\alpha_{pdw}) = 90°$. The $\eta_{pdw}$ calculated at selected values of $Re$ and $S_{pdw}$. At$S_{pdw} = 0$ mm, the computed value of $\eta_{pdw}$ is 3.14 which is more than unity. So the maximum $\eta_{pdw}$ suggest that the optimum value of spacer length of the PDWs is 0 mm. At optimum value of spacer length$S_{pdw} = 0$ mm, $\eta_{pdw}$ also attains maximum value.

## 4. Conclusions

In present investigation, experiments are carried out to investigate impact of perforated delta shaped winglets on $Nu_{rs}$ and $f_{rs}$ of SAH. The experimental data obtained on $Nu_{pdw}$ and $f_{rpdw}$ have analyzed to optimize the parameters of PDWs based on thermal performance considerations. The current study on artificially roughened SAH (PDWs on absorber plate of solar air heater) concludes;

- The comparative analysis of data obtained on temperature rise and pressure drop across the channel for SAH with PDWs and for SAH with smooth absorber plate reveals improvement in $Nu_{pdw}$.
- The perforated delta shaped winglets with spacer length $S_{pdw} = 0$ mm results in high $Nu_{pdw}$ and $f_{rpdw}$ as compared with other values of$S_{pdw}$.
- The $Nu_{pdw}$ and $f_{rpdw}$of roughened solar air heater with perforated delta shaped winglets was improvedby 5.17 and 4.52 times compared to the SAH with smooth absorber plate.
- The present perforated delta shaped winglets provide the highest $\eta_{pdw}$ of 3.14 at$S_{pdw} = 0$ mm and $Re$ of 12000.

## Declaration of Competing Interest

The authors declare that they have no known competing financial interests or personal relationships that could have appeared to influence the work reported in this paper.

## Appendix. -A

*Uncertainty study*

When the value of a factor is calculated by intentionally applying some dignified quantities, the error during the computation of z is provided using following equation:

$$\frac{\delta z}{z} = \left[\left(\frac{\delta z}{\delta u_1}\times\delta u_1\right)^2 + \left(\frac{\delta z}{\delta u_2}\times\delta u_2\right)^2 + \left(\frac{\delta z}{\delta u_3}\times\delta u_3\right)^2 + \cdots\cdots + \left(\frac{\delta z}{\delta u_n}\times\delta u_n\right)^2\right]^{1/2}$$

Here, $\delta u_1, \delta u_2, \delta u_3 \cdots\cdots\cdots .., \delta u_n$ represents probable errors during $u_1, u_2, u_3 \cdots\cdots\cdots, u_n$ measurements. Moreover,$\delta y$ is expressed as absolute uncertainty and $\frac{\delta z}{z}$ is represented as relative uncertainty. The range of determined uncertainty errors in parameters for tentative data is listed in Table A1. Equations selected for present uncertainty analysis are provided as follow:

### Uncertainty in Nusselt number ($Nu_{pdw}$)

$$Nu_{pdw} = \frac{h_{pdw}D_{hd}}{K_a}$$

$$\frac{\delta Nu_{pdw}}{Nu_{pdw}} = \left[\left(\frac{\delta D_{hd}}{D_{hd}}\right)^2 + \left(\frac{\delta h_{pdw}}{h_{pdw}}\right)^2 + \left(\frac{\delta K_a}{K_a}\right)^2\right]^{0.5}$$

### Uncertainty in Reynolds number (Re)

$$Re = \frac{V.D_{hd}}{v} = \frac{\rho_a V D_{hd}}{\mu}$$

$$\frac{\delta Re}{Re} = \left[\left(\frac{\delta D_{hd}}{D_{hd}}\right)^2 + \left(\frac{\delta V}{V}\right)^2 + \left(\frac{\delta \rho_a}{\rho_a}\right)^2 + \left(\frac{\delta \mu}{\mu}\right)^2\right]^{0.5}$$

**Table A1** Range of determined uncertainty errors in parameters for tentative data.

| Parameters description | Symbols | Unit | Uncertainty error (%) |
|---|---|---|---|
| Mass flow rate | $(m_{pdw})$ | $kg/sec$ | 1.357–2.124 |
| Heat transfer coefficient | $(h_{pdw})$ | $W/m^2K$ | 2.549–3.688 |
| Reynolds number | $(Re)$ | dimensionless | 1.64–3.27 |
| Nusselt number | $(Nu_{pdw})$ | dimensionless | 2.468–4.557 |
| Friction factor | $(f_{rpdw})$ | dimensionless | 1.342–2.231 |
| Thermohydraulic performance parameter $(\eta_p)$ | $\eta_{pdw}$ | dimensionless | 3.675–5.221 |

**Uncertainty in friction factor ($f_{pdw}$)**

$$f_{rpdw} = \frac{2(\Delta_p)_d D_{hd}}{4\rho_a L_{pdw} V^2}$$

$$\frac{\delta f_{rpdw}}{f_{rpdw}} = \left[\left(\frac{\delta D_{hd}}{D_{hd}}\right)^2 + \left(\frac{\delta V}{V}\right)^2 + \left(\frac{\delta L_{pdw}}{L_{pdw}}\right)^2 + \left(\frac{\delta \rho_a}{\rho_a}\right)^2 + \left(\frac{\delta(\Delta_p)_d}{(\Delta_p)_d}\right)^2\right]^{0.5}$$

**Uncertainty in thermohydraulic performance parameter ($\eta_{pdw}$)**

$$\eta_{pdw} = (Nu_{pdw}/Nu_{ss})/(f_{rpdw}/f_{ss})^{0.33}$$

$$\frac{\delta \eta_{pdw}}{\eta_{pdw}} = \left[\left(\frac{\delta Nu_{pdw}}{Nu_{pdw}}\right)^2 + \left(\frac{\delta f_{rpdw}}{f_{rpdw}}\right)^2\right]^{0.5}$$

## References


[1] A. Chel, G. Kaushik, Renewable energy technologies for sustainable development of energy efficient building, Alexandria Engineering Journal 57 (2018) 655–669.

[2] S.M. Dawoud, Developing different hybrid renewable sources of residential loads as a reliable method to realize energy sustainability, Alexandria Engineering Journal 60 (2021) 2435–2445.

[3] A. Singhy, R. Thakur, R. Kumar, Experimental analysis for co-generation of heat and power with convex lens as SOE and linear Fresnel Lens as POE using active water stream, Renewable Energy 163 (2021) 740–754.

[4] Z.S. Kareem, M.N.M. Jaafar, T.M. Lazim, S. Abdullah, A.F. AbdulWahid, Heat transfer enhancement in two-start spirally corrugated tube, Alexandria Engineering Journal 54 (2015) 415–422.

[5] S. Chamoli, ANN and RSM approach for modeling and optimization of designing parameters for a V down perforated baffle roughened rectangular channel, Alexandria Engineering Journal 54 (2015) 429–446.

[6] H.U. Warrier, V. Kotebavi, Numerical study of heat transfer enhancement in solar air heater duct fitted with delta winglets, Indian Journal of Science and Technology 9 (2016) 1–6.

[7] R. Maithani, A. Silori, J. Rana, S. Chamoli, Numerical analysis of heat transfer and fluid flow of a wavy delta winglets in a rectangular duct, Thermal Science and Engineering Progress 2 (2017) 15–25.

[8] P. Promvonge, C. Khanoknaiyakarn, S. Kwankaomeng, C. Thianpong, Thermal behavior in solar air heater channel fitted with combined rib and delta-winglet, Int. Commun. Heat Mass Transfer 38 (2011) 749–756.

[9] P. Promvonge, S. Skullong, Enhanced heat transfer in rectangular duct with punched winglets, Chin. J. Chem. Eng. 28 (2020) 660–671.

[10] J.S. Sawhney, R. Maithani, S. Chamoli, Experimental investigation of heat transfer and friction factor characteristics of solar air heater using wavy delta winglets, Appl. Therm. Eng. 117 (2017) 740–751.

[11] S. Singh, A. Singh, S. Chander, Thermal performance of a fully developed serpentine wavy channel solar air heater, J. Storage Mater. 25 (2019) 100896.

[12] S. Skullong, P. Promvonge, C. Thianpong, M. Pimsarn, Thermal performance in solar air heater channel with combined wavy-groove and perforated-delta wing vortex generators, Appl. Therm. Eng. 100 (2016) 611–620.

[13] S. Skullong, P. Promthaisong, P. Promvonge, C. Thianpong, M. Pimsarn, Thermal performance in solar air heater with perforated-winglet-type vortex generator, Sol. Energy 170 (2018) 1101–1117.

[14] H.U. Warrier, V.M. Kotebavi, Heat transfer enhancement in solar air heater duct fitted with punched hole delta winglets. IOP Conf. Series, Materials Science and Engineering 149 (2016) 012225.

[15] T. Chompookham, C. Thianpong, S. Kwankaomeng, P. Promvonge, Heat transfer augmentation in a wedge-ribbed channel using winglet vortex generators, Int. Commun. Heat Mass Transfer 37 (2010) 163–169.

[16] K. Torii, K.M. Kwak, K. Nishino, Heat transfer enhancement accompanying pressure loss reduction with winglet type vortex generators for fin tube heat exchangers, Int. J. Heat Mass Transf. 45 (2002) 3795–3801.

[17] K. Yakut, B. Sahin, C. Celik, N. Alemdaroglu, A. Kurnuc, Effect of tapes with double sided delta winglets on heat and vortex characteristics, Appl. Energy 80 (2005) 77–95.

[18] S. Skullong, C. Thianpong, N. Jayranaiwachira, P. Promvonge, Experimental and numerical heat transfer investigation in turbulent square-duct flow through oblique horseshoe baffles, Chem. Eng. Process. 99 (2016) 58–71.

[19] I. Kotcioglu, S. Caliskan, A. Cansiz, S. Baskaya, Second law analysis and heat transfer in a cross-flow heat exchanger with a new winglet type vortex generator, Energy 35 (2010) 3686–3895.

[20] S. Eiamsa-ard, K. Wongcharee, P. Eiamsa-ard, C. Thianpong, Heat transfer enhancement in a tube using delta winglet twisted tapes inserts, Appl. Therm. Eng. 30 (2010) 310–318.

[21] E.A. Handoyo, D. Ichsani, Sutardi Prabowo, Numerical studies on the effect of delta-shaped obstacles' spacing on the heat transfer and pressure drop in v-corrugated channel of solar air heater, Sol. Energy 131 (2016) 47–60.

[22] M. Ghalambaz, S.A.M. Mehryan, N. Mashoofi, A. Hajjar, A.J. Chamkha, M. Sheremet, O. Younis, Free convective melting-solidification heat transfer of nano-encapsulated phase change particles suspensions inside a coaxial pipe, Adv. Powder Technol. 31 (2020) 4470–4481.

[23] S.M.H. Zadeh, S.A.M. Mehryan, M. Ghalambaz, M. Ghodrat, J. Young, A. Chamkha, Hybrid thermal performance enhancement of a circular latent heat storage system by utilizing partially filled copper foam and Cu/GO nano-additives, Energy 213 (2020) 118761.

[24] M. Ghalambaz, S.A.M. Mehryan, I. Zahmatkesh, A. Chamkha, Free convection heat transfer analysis of a suspension of nano-encapsulated phase change materials (NEPCMs) in an inclined porous cavity, Int. J. Therm. Sci. 157 (2020) 106503.

[25] S.A.M. Mehryan, M. Ghalambaz, A.J. Chamkha, M. Izadi, Numerical study on natural convection of Ag-MgO hybrid/water nanofluid inside a porous enclosure: A local thermal non-equilibrium model, Powder Technol. 367 (2020) 443–455.

[26] M. Ghalambaz, A. Doostani, E. Izadpanahi, A.J. Chamkha, Conjugate natural convection flow of Ag–MgO/water hybrid nanofluid in a square cavity, J. Therm. Anal. Calorim. 139 (2020) 2321–2336.

[27] A.J. Chamkha, Solar radiation assisted natural convection in uniform porous medium supported by a vertical flat plate, J. Heat Transfer 119 (1997) 89–96.

[28] S. Parvin, R. Nasrin, M.A. Alim, N.F. Hossain, A.J. Chamkha, Thermal conductivity variation on natural convection flow of water-alumina nanofluid in an annulus, Int. J. Heat Mass Transf. 55 (2012) 5268–5274.

[29] A.J. Chamkha, H.S. Takhar, V.M. Soundalgekar, Radiation effects on free convection flow past a semi-infinite vertical plate with mass transfer, Chem. Eng. J. 84 (2001) 335–342.

[30] A.M. Manokar, M. Vimala, R. Sathyamurthy, A.E. Kabeel, D. P. Winston, A.J. Chamkha, Enhancement of potable water production from an inclined photovoltaic panel absorber solar

still by integrating with flat-plate collector, Environ. Dev. Sustain. 22 (2020) 4145–4167.
[31] H.T. Basha, R. Sivaraj, A.S. Reddy, A.J. Chamkha, SWCNH/diamond-ethylene glycol nanofluid flow over a wedge, plate and stagnation point with induced magnetic field and nonlinear radiation-solar energy application, The European Physical Journal Special Topics 228 (2019) 2531–2551.
[32] C. Sasikumar, A.M. Manokar, M. Vimala, D.P. Winston, A.E. Kabeel, R. Sathyamurthy, A.J. Chamkha, Experimental studies on passive inclined solar panel absorber solar still, J. Therm. Anal. Calorim. 139 (2020) 3649–3660.
[33] S. Paraschiv, N. Bărbuţă-Mişu, L.S. Paraschiv, Technical and economic analysis of a solar air heating system integration in a residential building wall to increase energy efficiency by solar heat gain and thermal insulation, Energy Rep. 6 (2020) 459–474.
[34] J. Long, K. Xia, H. Zhong, H. Lu, A. Yongga, Study on energy-saving operation of a combined heating system of solar hot water and air source heat pump, Energy Convers. Manage. 229 (2021) 113624.
[35] H.M. Teamah, Comprehensive review of the application of phase change materials in residential heating applications, Alexandria Engineering Journal 60 (2021) 3829–3843.
[36] H.A.M. Teamah, M.F. Lightstone, J.S. Cotton, Numerical investigation and nondimensional analysis of the dynamic performance of a thermal energy storage system containing phase change materials and liquid water, J. Sol. Energy Eng. 139 (2017) 021004.
[37] H.M. Teamah, M.F. Lightstone, Numerical study of the electrical load shift capability of a ground source heat pump system with phase change thermal storage, Energy Build. 199 (2019) 235–246.
[38] R. Kumar, A. Kumar, A. Sharma, R. Chauhan, M. Sethi, Experimental study of heat transfer enhancement in a rectangular duct distributed by multi-V-perforated baffle of different relative baffle width, Heat Mass Transfer 53 (2017) 1289–1304.
[39] A. Kumar, R. Kumar, R. Chauhan, M. Sethi, A. Kumari, N. Verma, R. Nadda, Single phase thermal and hydraulic performance analysis of a V-pattern dimpled obstacles air passage, Exp. Heat Transfer 39 (2017) 393–426.
[40] A. Kumar, R. Kumar, R. Maithani, R. Chauhan, S. Kumar, R. Nadda, An experimental study of heat transfer enhancement in an air channel with broken multi type V-baffles, Heat Mass Transfer 53 (2017) 3593–3612.
[41] R. Nadda, A. Kumar, R. Maithani, R. Kumar, Investigation of thermal and hydrodynamic performance of impingement jets solar air passage with protrusion with combination arc obstacle on the heated plate, Exp. Heat Transfer 31 (2018) 232–250.
[42] R. Kumar, R. Chauhan, M. Sethi, A. Kumar, Experimental investigation on overall thermal performance of fluid flow in a rectangular channel with discrete V-pattern baffle, Thermal Science 22 (2018) 183–191.
[43] R. Kumar, R. Nadda, A. Rana, R. Chauhan, S.S. Chandel, Performance investigation of a solar thermal collector provided with air jets impingement on multi-V-shaped protrusion ribs absorber plate, Heat Mass Transfer 56 (2020) 913–930.
[44] R.P. Benedict, Fundamental of temperature pressure and flow measurements, third edition., Wiley-Interscience Publication, New York, 1984.
[45] A. Kumar, R.P. Saini, J.S. Saini, Experimental investigation on heat transfer and fluid flow characteristics of air flow in a rectangular duct with Multi v-shaped rib with gap roughness on the heated plate, Sol. Energy 86 (2012) 1733–1749.
[46] S.J. Klein, A. McClintock, The description of uncertainties in a single sample experiments, Mechanical Engineering 75 (1953) 3–8.
[47] M.J. Lewis, Optimizing the thermohydraulic performance of rough surfaces, Int. J. Heat Mass Transf. 18 (1975) 1243–1248.